Adaptive Stabilization of a Permanent Magnet Synchronous Generator-Based DC Electrical Power System in More Electric Aircraft

Apichai Suyapan, Kongpan Areerak, *Member*, *IEEE*, Serhiy Bozhko, *Senior Member*, *IEEE*, Seang Shen Yeoh, and Kongpol Areerak

***Abstract*—Most loads of electrical power system on a more electric aircraft (MEA) are regulated power converters. These loads behave as constant power loads that can significantly affect system stability. The system will become unstable and will be unable to operate at the rated power. In this paper, a novel adaptive stabilization of a permanent magnet synchronous generator-based DC electrical power system in MEA is presented using a nonlinear feedback approach via loop-cancellation technique with a simple equation of feedback gain, which can be calculated from the power level of the constant power load. The equation can be derived from a polynomial curve fitting based on the proposed mathematical model derived using the *dq* method. The adaptive stabilization results are validated by small-signal stability analysis using the linearization technique, large-signal stability analysis using the phase plane analysis, intensive time-domain simulation using MATLAB and experimentation. The results indicate that the proposed adaptive stabilization technique can provide the considered aircraft power system always stable for all operating conditions within the rated power and the DC bus voltage can adhere to the MIL-STD-704F standard.**

***Index Terms*—Adaptive Stabilization, Nonlinear Feedback, Loop-Cancellation Technique, More Electric Aircraft (MEA), Constant Power Load (CPL), Small-Signal Stability Analysis, Large-Signal Stability Analysis, *dq* Model.**

I. Introduction

The more electric aircraft (MEA) is an essential concept and tendency in modern aerospace engineering that attempts to replace four sub-systems, i.e., electrical, pneumatic, hydraulic, and mechanical systems with only an electrical system. The aim of using MEA is to reduce operating costs, fuel consumption, environmental impact, and overall weight. Furthermore, improvement in the efficiency and reliability of overall aircraft systems has been concerned. AC distribution system is the preferred system for use in MEA, whereas a hybrid distribution system serves as a second option. However, at present (and in the future), a DC distribution system represents a potential architecture for MEA because of the distribution advantages it presents. These include higher system efficiency and reliability, as well as lower overall weight and power losses due to the absence of reactive power compensation equipment [1-6].

The concept and tendency of MEA have resulted in the wide use of power electronic technology because it is easy to control and has high efficiency and low maintenance costs. Hence, the electrical power system loads on MEA typically include regulated power converters, e.g., power converters that are connected to an electric motor to control the current and speed of the motor as well as AC/DC or DC/DC converters with their output voltage controllers. However, regulated power converters behave as constant power loads (CPLs), which are characterized as having negative impedance to overall systems [6-8]. These CPLs can significantly affect the system stability. Instability in this regard may affect controller performance or cause system damage [6, 8, and 9]. Thus, stability analysis for an electrical system with CPLs is important and necessary, particularly for the electrical power systems on MEA. System instability on MEA not only affects the controller performance but may also cause damage to the overall system, which, consequently, will impact passenger safety. These are all undesirable circumstances in the context of aviation. From past to present research, stability studies have been proposed to predict unstable points that can be used to avoid unstable operation. However, stability results alone cannot revert an unstable system to stable system. Therefore, instability mitigation issues have been reviewed to extend system operation.

The basic concept of instability mitigation due to CPL involves the compensation or elimination of the CPL effect by increasing the system damping. These can be categorized into two methods, i.e., passive and active damping. The passive approach [10 and 11] involves hardware modification by increasing filter capacitance, decreasing filter inductance, or adding a passive component, e.g., a resistor, a resistor with a capacitor, or a resistor with an inductor to the system to increase system damping, resulting in increased system stability. Passive damping involves a simple method for design and practical

This work was supported by the Thailand Research Fund (TRF), the Royal Golden Jubilee Ph.D. Program (RGJ: grant number PHD/0089/2560) and by Suranaree University of Technology (SUT), THAILAND and Institute for Aerospace Technology (IAT), University of Nottingham (UoN), UK. *(Corresponding author: Kongpan Areerak).*

A. Suyapan, K-N. Areerak and K-L. Areerak are with the School of Electrical Engineering, Institute of Engineering, Suranaree University of Technology, Nakhon Ratchasima, 30000, THAILAND (e-mail: japichaisuyapan@gmail.com; kongpan@sut.ac.th; kongpol@sut.ac.th).

S. Bozhko and S.S. Yeoh are with the Department of Electrical and Electronic Engineering, University of Nottingham, Nottingham, NG7 2RD, UK (email: serhiy.bozhko@nottingham.ac.uk; seang.yeoh@nottingham.ac.uk).

This article has been accepted for publication in a future issue of this journal, but has not been fully edited. Content may change prior to final publication. Citation information: DOI 10.1109/TTE.2021.3081161, IEEE Transactions on Transportation Electrification

implementations. However, the drawbacks of such damping are an increase in the overall system size, weight, and price and system power losses, which result in decreased system performance. Active damping [11-12, 13-26] is an approach based on control structure modifications. A compensation signal, known as a stabilizing signal, is created and introduced to existing control structures. Virtual system damping can also be created to increase system stability in which the active damping approach is not a hardware modification. In this way, the system can achieve higher efficiency and reliability compared with using a passive damping technique. Most of current research thus tends to use the active damping approach for instability mitigation. According to feedback characteristics, active damping can be divided into two methods. The first is the linear feedback method [11-12, 14-17, 19-23], in which the creation of the compensation signal is based on the virtual impedance principle. However, research [11, 13, and 26] reported that linear feedback compensates only for a limited amount of CPL [11, 13, 18 and 26]. The second approach, the nonlinear feedback method, can eliminate a wide range of CPLs. The compensation signal is designed using a nonlinear control technique, e.g., sliding mode control, state space poles placement, a loop-cancellation technique, and neural networks [11, 13, 18, 24-26].

The active damping approach can be implemented in three ways as given in Table I. The first is by implementing modification at the feeder or source side [10-17 and 22]. The advantage of this approach is that it does not affect the load performance. The main primary disadvantage, however, is a limitation in terms of a usable system. This method can only be used for a feeder system with switched converters. When the feeder system includes non-switched converters, such as an uncontrolled rectifier, CPL compensation at the feeder side is not possible. In this case, a second approach, i.e., modification at the load or CPL side [11, 18-21, 23-25] can be used. Modification at the CPL side is a method that can compensate for the CPL effect directly by introducing a compensation signal to the existing control loop. The drawback of this method is that the load performance will be reduced. If the load performance becomes more important than the losses, compensation using an additional auxiliary circuit is a suitable option [11 and 26], in which an auxiliary circuit is installed between the feeder and load systems. This will, however, increase the cost and complexity of the overall system, as well as power loss.

TABLE I
THE ADVANTAGES AND LIMITATIONS OF MITIGATION METHODS

Method	Advantages	Limitations
Feeder Side Active Damping [10-17 and 22]	not affect to load performance	can only be applied for the switched converters
CPL Side Active Damping [11, 18-21, 23-25]	can compensate CPL effect directly	affect the load performance
Active Damping using Auxiliary Circuits [11 and 26]	can be applied for the non-switched converters without the load performance effect	increase cost, power loss, and complexity of the overall system

On the basis of the advantage of the nonlinear feedback technique, this paper presents adaptive stabilization using the loop-cancellation technique. The compensating signal is introduced into the existing control loop at the source side. Additionally, the stabilization gain can be adopted based on the system's operating point to maintain system stability. The simple equation derived from a polynomial curve fitting, alongside the instability line provided by the proposed averaging model, is used to update the stabilization gain. After applying the proposed mitigation technique, the considered MEA system will always be stable within the rated operating point. Furthermore, when stabilization is achieved, the DC bus voltage can adhere to the MIL-STD-704F standard [27]. The intensive time-domain simulation using MATLAB and the experimental results were used to validate the theoretical results.

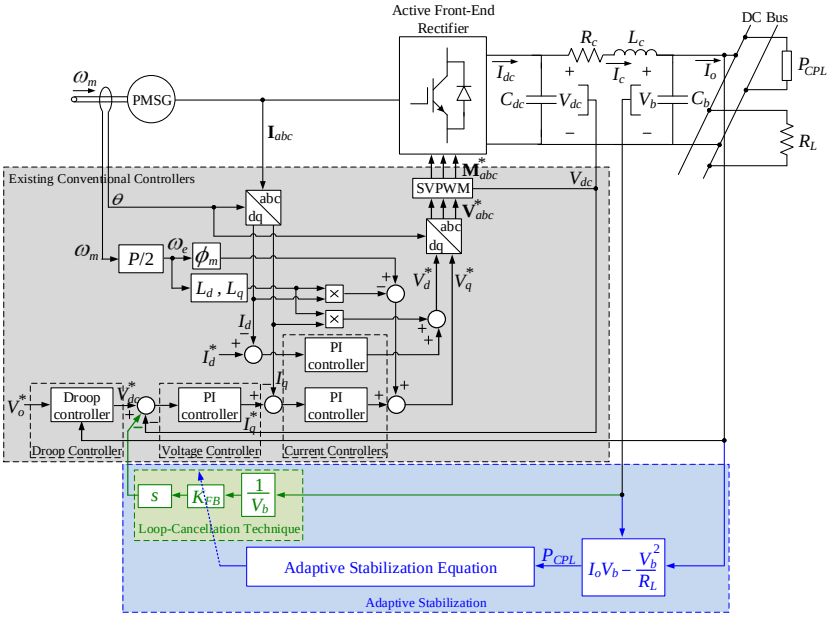

Fig. 1. The considered MEA power system.

This paper is structured as follows; In Section II, a single-generator-single-bus DC distribution MEA power system with the loop-cancellation technique is introduced. Applying the loop-cancellation technique to the considered MEA and deriving the mathematical model using the *dq* method is also explained. In Section III, a review of system stability is presented by small-signal stability analysis using the eigenvalue theorem and large-signal stability analysis using the phase plane analysis. The details of the proposed adaptive stabilization are addressed in Section III. The validation of the theoretical analysis by simulation using MATLAB and of the experiment using a test rig built in the laboratory are presented in Section IV. Finally, the advantages and benefits of the proposed adaptive stabilization approach, as well as future research, are concluded and discussed in Section V.

II. The Considered More Electric Aircraft Power System with The Loop-Cancellation Technique

Fig. 1 shows the MEA power system considered in this paper. It comprises a permanent magnet synchronous generator (PMSG), which is used to generate AC power by converting mechanical power from the aircraft's engine turbines to electrical power. An active front-end (AFE) rectifier is used to convert the AC power from the PMSG to DC power for all MEA loads, whereas a DC-link capacitor is used to reduce the ripple voltage of the DC bus to obtain a smoother and more constant voltage. Furthermore, the DC transmission line and all MEA loads including the CPL referred to the regulated power converters, resistive load represented to a wing de-icing system and capacitor bank. The controllers of the AFE rectifier, indicated by the gray area in Fig. 1, are the vector controllers on the *dq*-axis. The current controller on the *d*-axis is used to control the PMSG and enable it to function at full-flux operation by setting I_d^* to 0. The current controller on the *q*-axis and the voltage controller are used to regulate the voltage across the DC-link capacitor (V_{dc}), which in this instance equals 250–280 V; this is based on the MIL-STD-704F standard [27], in which the nominal voltage (V_o^*) is set to 270 V. The droop controller is used to control current or power sharing from each PMSG for all MEA loads to obtain the desired V-I droop characteristic. The output of the droop controller is the reference voltage for the V_{dc} controller (V_{dc}^*). Furthermore, Fig. 1 indicates nonlinear feedback via the loop-cancellation technique and the adaptive stabilization approach (the green and blue areas, respectively, in Fig. 1). In this section, only the considered MEA with the loop-cancellation technique is studied. The adaptive stabilization approach will be described in Section III.

As shown in Fig. 1, the instability mitigation technique is added to the existing conventional controllers. The application of the loop-cancellation technique for instability mitigation of the considered MEA is explained as follows:

The *dq* method is applied for deriving the mathematical model with which to obtain a time-invariant model suitable for a stability study. The assumptions for deriving the model are that the AFE rectifier is operated under the continuous conduction mode (CCM), an overlap angle (μ) below 60°, and all harmonics in the system are ignored.

For model derivation, the considered MEA system can be divided into three parts.

A. The Permanent Magnet Synchronous Generator Model

The dynamic equations of the PMSG on *dq* frame with a synchronously rotating reference frame [4, 5] are shown in (1).

$$\begin{cases} \dot{I}_d = -\dfrac{R_s}{L_d} I_d + \dfrac{\omega_e L_q}{L_d} I_d - \dfrac{1}{L_d} V_d \\ \dot{I}_q = -\dfrac{\omega_e L_d}{L_q} I_d - \dfrac{R_s}{L_q} I_q - \dfrac{1}{L_q} V_q + \dfrac{\omega_e \phi_m}{L_q} \end{cases} \tag{1}$$

where R_s is the stator resistance, L_d and L_q are the inductance on *dq*-axis, ϕ_m is the permanent magnet flux linkage, ω_e is the electrical rotor angular velocity, I_d and I_q are the stator current on *dq*-axis, and V_d and V_q are the stator voltage on *dq*-axis.

B. The AFE Rectifier Model

The inner structure of the AFE rectifier includes six switches, herein identified as insulated-gate bipolar transistors (IGBTs). After using the *dq* method to eliminate the IGBTs' switching behaviors, the AFE rectifier can be represented by a transformer on the *dq*-axis with the ratios M_d:1 and M_q:1 [4-6]. The time-invariant switching function of the AFE rectifier is shown in (2).

$$\begin{cases} M_d = \dfrac{m}{2}\cos(\phi - \phi_{con.}) \\ M_q = -\dfrac{m}{2}\sin(\phi - \phi_{con.}) \end{cases} \tag{2}$$

where m is the modulation index, ϕ is the phase angle of *dq*-axis and $\phi_{con.}$ is the phase angle of voltage vector at the converter bus.

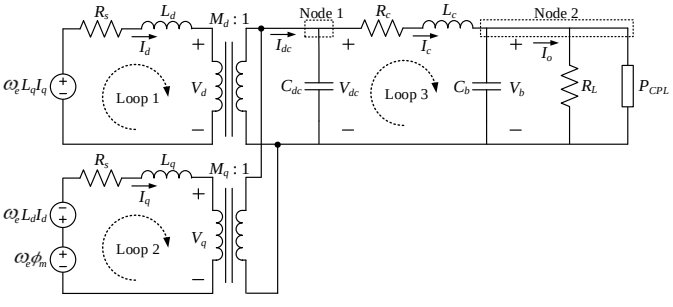

Fig. 2. The equivalent circuit on the *dq*-axis of the considered MEA power system without the controllers.

First, the open loop control of the AFE rectifier is considered. According to (1) and (2), as well as setting the *dq*-axis rotating at the PMSG rotor angle, the considered MEA without the closed-loop control can be represented by the equivalent circuit on the *dq*-axis as shown in Fig. 2. After analyzing the equivalent circuit in Fig. 2 using Kirchhoff's voltage law

and Kirchhoff's current law, a mathematical model of the considered MEA without controllers is given in (3).

$$\begin{cases} \dot{I}_d = -\dfrac{R_s}{L_d} I_d + \omega_e I_q - \dfrac{M_d}{L_d} V_{dc} \\ \dot{I}_q = -\omega_e I_d - \dfrac{R_s}{L_q} I_q - \dfrac{M_q}{L_q} V_{dc} + \dfrac{\omega_e \phi_m}{L_q} \\ \dot{V}_{dc} = \dfrac{3M_d}{2C_{dc}} I_d + \dfrac{3M_q}{2C_{dc}} I_q - \dfrac{1}{C_{dc}} I_c \\ \dot{I}_c = \dfrac{1}{L_c} V_{dc} - \dfrac{R_c}{L_c} I_c - \dfrac{1}{L_c} V_b \\ \dot{V}_b = \dfrac{1}{C_b} I_c - \dfrac{1}{R_L C_b} V_b - \dfrac{P_{CPL}}{C_b V_b} \end{cases} \tag{3}$$

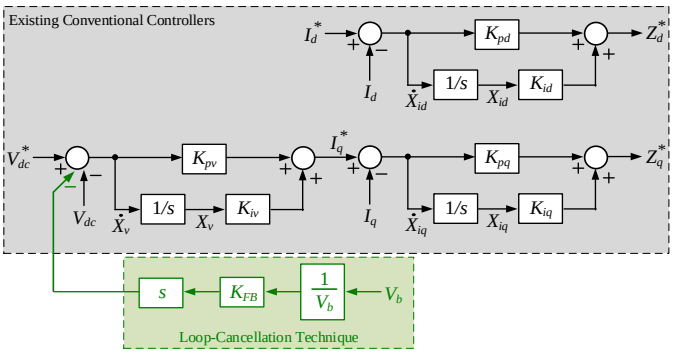

Fig. 3. A block diagram of the controllers without the adaptive stabilization.

C. Controller Models

Fig. 3 shows a block diagram of the AFE rectifier controllers without adaptive stabilization. It includes the existing conventional controllers as shown in the gray area. The details for how to design the controllers can be found in [4 and 5]. The green area is the loop-cancellation for instability mitigation.

Referring to (3), the CPL effect is represented by the term $\frac{P_{CPL}}{V_b}$ in the differential equation V_b. This effect can degrade the system stability. Hence, the instability mitigation via the loop-cancellation technique for the considered MEA is required to ensure that the MEA system can be operated within all ranges under the rated. The mitigation is started by detecting the voltage across the capacitor bank (V_b). Then, V_b is inverted and multiplied by feedback gain K_{FB} as shown by the green area in Fig. 3. The gain can be adjusted to achieve a suitable value for eliminating the CPL effect. After considering (3) in the steady-state by setting all differential equations to 0 ($\dot{\mathbf{x}} = 0$), the relationship between V_{dc} and V_b is given in (4), which indicates that the CPL effect has a plus sign. Consequently, the elimination of the CPL effect via the V_{dc} controller can be achieved by creating a stabilizing signal in the V_{dc} control loop with a minus sign. Thus, a voltage sensor is required only for V_b. Consequently, this does not impact power loss or the size, weight, and cost of the overall system.

$$V_{dc} = \left(1 + \frac{R_c}{R_L}\right) V_b + \frac{R_c P_{CPL}}{V_b} \tag{4}$$

After analyzing the control structure in Fig. 3, equations for the controllers are given in (5), and the reference modulation index on the *dq*-axis ($\mathbf{M}_{dq}^*$) can be calculated by (6). As shown by (5), the new state variables, i.e., X_v, X_{id}, and X_{iq} are obtained when the controllers are considered. Here, X_v, X_{id}, and X_{iq} are from the V_{dc}, I_d, and I_q control loops, respectively.

$$\begin{cases} Z_d^* = -K_{pd} I_d + K_{id} X_{id} + K_{pd} I_d^* \\ Z_q^* = -K_{pq} I_q - K_{pv} K_{pq} V_{dc} + K_{iv} K_{pq} X_v + K_{iq} X_{iq} \\ \qquad + K_{pv} K_{pd} V_{dc}^* - K_{pv} K_{pq} K_{FB} \dfrac{d}{dt}\left(\dfrac{1}{V_b}\right) \end{cases} \tag{5}$$

with $V_{dc}^* = V_o^* - K_D \left(\dfrac{V_b}{R_L} + \dfrac{P_{CPL}}{V_b}\right)$

$$\begin{cases} M_d^* = \left(\dfrac{1}{V_{dc}}\right)(Z_d^* + \omega_e L_q I_q) \\ M_q^* = \left(\dfrac{1}{V_{dc}}\right)(Z_q^* - \omega_e L_d I_d + \omega_e \phi_m) \end{cases} \tag{6}$$

$$\dot{I}_{q1} = \dot{I}_q - \frac{K_{pv} K_{pq} K_{FB}}{L_q} \frac{d}{dt}\left(\frac{1}{V_b}\right) \tag{7}$$

Creating the new state variable $\dot{I}_{q1}$ as defined by (7) can be applied to eliminate term $\frac{d}{dt}\left(\frac{1}{V_b}\right)$, which can simplify the model. Deriving the mathematical model for the considered MEA (Fig. 1) can be performed by substituting M_d and M_q in (3) with M_d^* and M_q^* from (5) and (6) and by substituting I_q in (3) with I_{q1} in (7). The mathematical model of the considered MEA power system with the loop-cancellation technique in Fig. 1, derived using the *dq* method, is given in (8). The time-invariant system model in (8) is thus a suitable model for studying system stability.

III. Stability Studies and Adaptive Stabilization

In this section, the considered system stability is reviewed using small-signal stability analysis via the linearization technique and large-signal stability analysis via the phase plane

This article has been accepted for publication in a future issue of this journal, but has not been fully edited. Content may change prior to final publication. Citation information: DOI 10.1109/TTE.2021.3081161, IEEE Transactions on Transportation Electrification

$$
\begin{cases}
\dot{I}_d = \left(\dfrac{K_{pd}-R_s}{L_d}\right) I_d - \dfrac{K_{id}}{L_d} X_{id} - \dfrac{K_{pd}}{L_d} I_d^* \\
\dot{I}_{q1} = \left(\dfrac{K_{pq}-R_s}{L_q}\right) I_{q1} + \dfrac{K_{pv}K_{pq}}{L_q} V_{dc} + \dfrac{K_{pv}K_{pq}K_D}{L_q R_L} V_b \\
\quad + \dfrac{K_{pv}K_{pq}K_D P_{CPL}}{L_q} \cdot \dfrac{1}{V_b} - \dfrac{K_{iv}K_{pq}}{L_q} X_v - \dfrac{K_{iq}}{L_q} X_{iq} \\
\quad - \dfrac{K_{pv}K_{pq}}{L_q} V_o + \dfrac{K_{pv}K_{pq}K_{FB}(K_{pq}-R_s)}{L_q^2} \cdot \dfrac{1}{V_b} \\
\dot{V}_{dc} = \dfrac{3}{2C_{dc}} \cdot \dfrac{1}{V_{dc}} [-K_{pd} I_d^2 + K_{id} I_d X_{id} + K_{pd} I_d I_d^* \\
\quad - K_{pq} I_{q1}^2 + \omega_e \phi_m I_{q1} - K_{pv} K_{pq} I_{q1} V_{dc} \\
\quad - \dfrac{K_{pv}K_{pq}K_D}{R_L} I_{q1} V_b + K_{iv} K_{pq} I_{q1} X_v + K_{iq} I_{q1} X_{iq} \\
\quad + K_{pv} K_{pq} I_{q1} V_o - (\dfrac{2K_{pv}K_{pq}^2 K_{FB}}{L_q} I_{q1} \\
\quad + \dfrac{K_{pv}^2 K_{pq}^3 K_{FB}^2}{L_q^2} \cdot \dfrac{1}{V_b} + K_{pv} K_{pq} K_D P_{CPL} I_{q1} \\
\quad + \dfrac{K_{pv}^2 K_{pq}^2 K_{FB}}{L_q} V_{dc} + \dfrac{K_{pv}^2 K_{pq}^2 K_D P_{CPL} K_{FB}}{L_q} \cdot \dfrac{1}{V_b} \\
\quad - \dfrac{K_{pv} K_{iv} K_{pq}^2 K_{FB}}{L_q} X_v - \dfrac{K_{pv} K_{pq} K_{iq} K_{FB}}{L_q} X_{iq} \\
\quad - \dfrac{K_{pv}^2 K_{pq}^2 K_{FB}}{L_q} V_o - \dfrac{\omega_e \phi_m K_{pv} K_{pq} K_{FB}}{L_q}) \dfrac{1}{V_b} \\
\quad - \dfrac{K_{pv}^2 K_{pq}^2 K_D K_{FB}}{L_q R_L}] - \dfrac{1}{C_{dc}} I_c \\
\dot{I}_c = \dfrac{1}{L_c} V_{dc} - \dfrac{R_c}{L_c} I_c - \dfrac{1}{L_c} V_b \\
\dot{V}_b = \dfrac{1}{C_b} I_c - \dfrac{1}{R_L C_b} V_b - \dfrac{P_{CPL}}{C_b V_b} \\
\dot{X}_v = -V_{dc} - \dfrac{K_D}{R_L} V_b - \dfrac{K_D P_{CPL}}{V_b} + V_o \\
\dot{X}_{id} = -I_d + I_d^* \\
\dot{X}_{iq} = -I_{q1} - K_{pv} V_{dc} - \dfrac{K_{pv} K_D}{R_L} V_b + K_{iv} X_v + K_{pv} V_o \\
\quad - (K_{pv} K_D P_{CPL} + \dfrac{K_{pv} K_{pq} K_{FB}}{L_q}) \cdot \dfrac{1}{V_b}
\end{cases} \tag{8}
$$

analysis for unstable point prediction. Additionally, instability mitigation is presented. The details for how to create adaptive stabilization based on the loop-cancellation technique for the considered MEA are also described.

The system model in (8) indicates that K_{FB} occurred in the equation. If K_{FB} is equal to 0, it infers the system is operated without the proposed mitigation technique. After linearizing (8) by first-order Taylor series, eigenvalues from the linearization of (8) were calculated. The system parameters (as given in the appendix) represent a scaled version due to laboratory limitations in the experimental setup. Using these parameters, Fig. 4(a) shows the dominant eigenvalue plot of the considered MEA system when P_{CPL} is varied from 0.8 to 2.2 kW without the mitigation technique (K_{FB} = 0). It is shown that the real roots of the dominant eigenvalues at P_{CPL} = 1.4 kW are higher than 0. Therefore, at this operating point, the system is unstable. The system instability occurs before the rated power in this instance reaches $P_{CPL(rated)} = 2.2$ kW. To return the system to a stable state, instability mitigation via the loop-cancellation technique is applied.

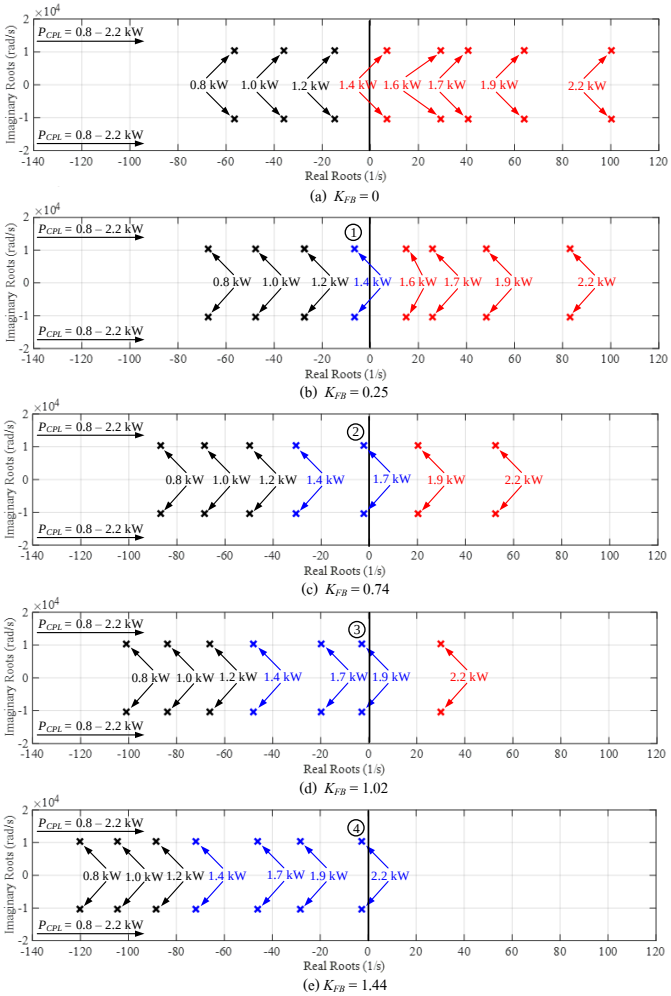

Fig. 4. Analytical results for the unstable point prediction and instability mitigation using the eigenvalue theorem.

Fig. 4(b) to Fig. 4(e) present the dominant eigenvalue plots of the considered MEA with the proposed mitigation technique when K_{FB} is equal to 0.25, 0.74, 1.02 and 1.44, respectively. Fig. 4(b) shows that the dominant eigenvalues at $P_{CPL} = 1.4$ kW (the unstable point) moved from the right-hand side to the left-hand side of the s-plane. This means that the proposed

mitigation technique can return the unstable system to a stable state by only increasing K_{FB} from 0 to 0.25. However, if the P_{CPL} is increased beyond 1.4 kW (here, it is 1.7 kW) while the K_{FB} remains fixed at 0.25, the gain will not be sufficient for mitigation. Accordingly, the system will become unstable again. To make the system stable at $P_{CPL}=1.7$ kW, K_{FB} should be increased to 0.74 (Fig. 4(c)). For P_{CPL} equal to 1.9 and 2.2 kW (rated power), K_{FB} should be increased to 1.02 and 1.44, respectively.

K_{FB} = 1.44 can be used to mitigate the system (Fig. 4), which can make the system stable for all load powers within the rated range. The phase plane analysis is used to investigate the DC bus voltage response (V_b) adherence to the MIL-STD-704F standard when the proposed mitigation technique is applied. Using the system model in (8) with the system parameters given in the appendix, the trajectory of the considered MEA on the I_c–V_b plane when $P_{CPL}=1.4$ kW without the mitigation technique (K_{FB} = 0) is determined (Fig. 5(a)). The system trajectory motion starts from the initial point and then diverges from the equilibrium point, indicating that the system is unstable at $P_{CPL}=1.4$ kW, corresponding to the eigenvalue theorem analysis in Fig. 4(a). Fig. 5(b) presents the system trajectory at $P_{CPL}=1.4$ kW when using $K_{FB}=1.44$ (the K_{FB} = 1.44 can stabilize the system for all load powers within the rated range). The analytical result shows that the trajectory can converge to the equilibrium point, indicating the system is stable at such conditions. However, the transient state V_b oscillates considerably exceeding the range of 200–330 V, as specified by the MIL-STD-704F standard. Moreover, the steady-state V_b is also not in the range of 250–280 V, as specified by the denoted standard. Fig. 6(b) shows the simulation results when P_{CPL} is increased from 1.2 to 1.4 kW with $K_{FB}=1.44$. The results show that the steady-state response of V_b does not adhere to the MIL-STD-704F standard with $K_{FB}=1.44$ for $P_{CPL}=1.4$ kW, corresponding to the analysis in Fig. 5(b). Based on the analysis in Fig. 5(c), the system trajectory at $P_{CPL}=1.4$ kW when $K_{FB}=0.25$ can converge to the equilibrium point, and the V_b responses in both transient and steady states can adhere to the standard. Fig. 6(a) shows the simulation results, confirming the analytical results of Fig. 5(c). Concordantly, $K_{FB}=0.25$ stabilizes the system for $P_{CPL}=1.4$ kW, and the V_b responses in both transient and steady states adhere to the MIL-STD-704F standard, while the undesirable V_b response is obtained for K_{FB} = 1.44. Hence,

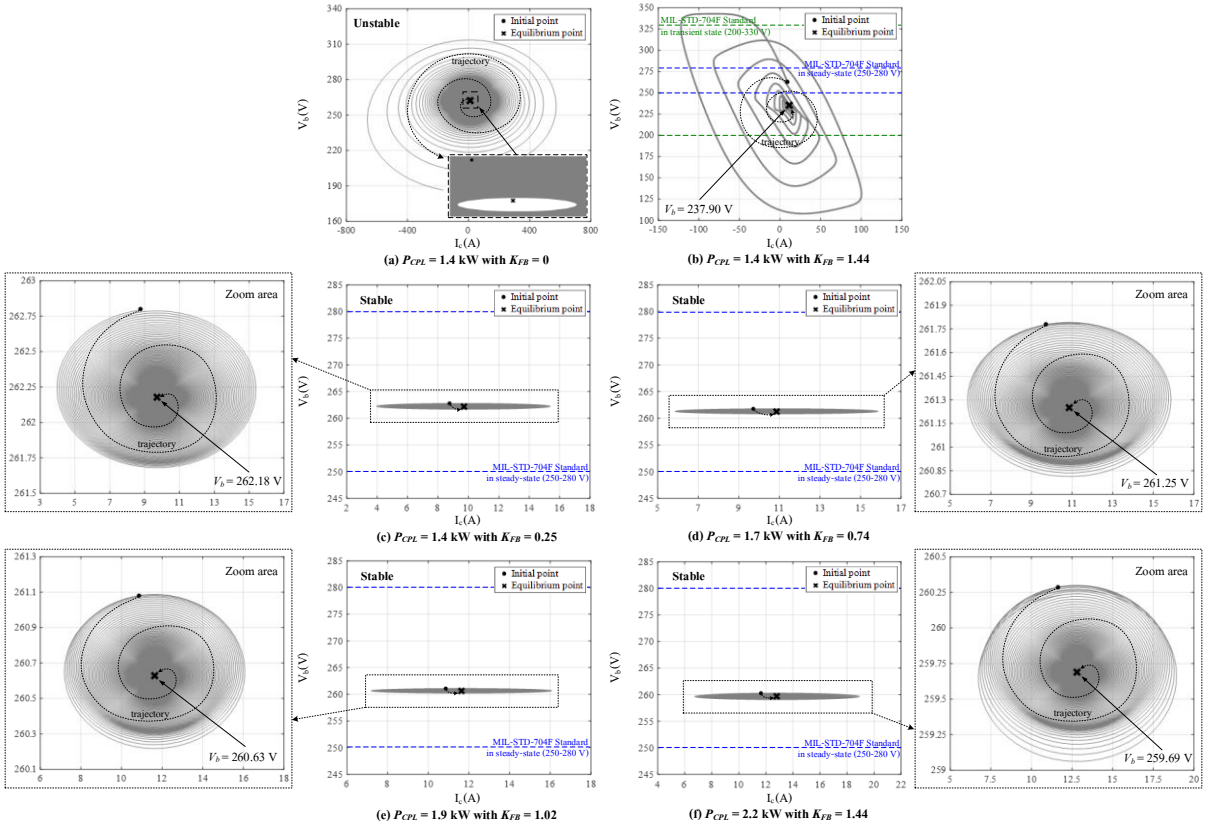

Fig. 5. Analytical results from the phase plane analysis.

This article has been accepted for publication in a future issue of this journal, but has not been fully edited. Content may change prior to final publication. Citation information: DOI 10.1109/TTE.2021.3081161, IEEE Transactions on Transportation Electrification

a high K_{FB} can cause the nonadherence of the V_b response to the standard. Therefore, the design of a suitable K_{FB} value is required. The phase plane analysis was also performed for other P_{CPLs}. Fig. 5 shows that $K_{FB} = 0.74$ is suitable for $P_{CPL} = 1.7$ kW (Fig. (d)), while $K_{FB} = 1.02$ and 1.44 are also appropriate for $P_{CPL} = 1.9$ kW (Fig. (e)) and 2.2 kW (Fig. (f)), respectively. Thus, K_{FB} must be designed sufficiently small to avoid undesirable V_b response. K_{FB} should be adopted based on the P_{CPL} level to ensure that the system remains stable for all operating conditions within the rated power. Hence, adaptive stabilization is proposed to provide the appropriate K_{FB}.

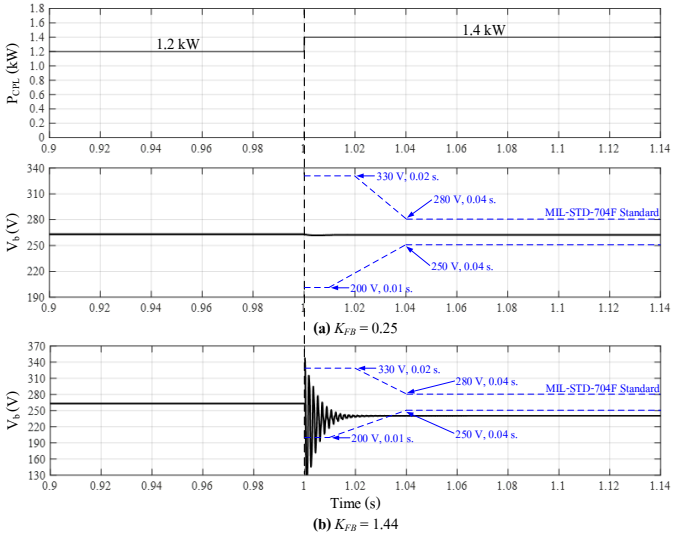

Fig. 6. Simulation results for instability mitigation at P_{CPL} = 1.4 kW.

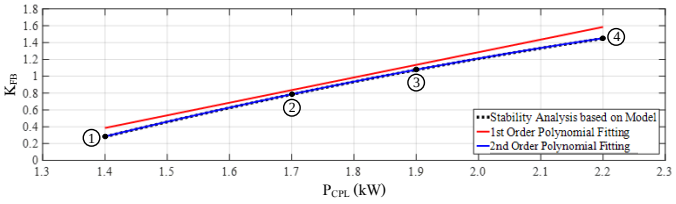

Fig. 7. Polynomial curve fitting.

The proposed adaptive stabilization is based on a simple equation obtained from polynomial curve fitting (Fig. 7). The instability line, indicated by the black dashed line in Fig. 7, is first calculated from the stability analysis via the proposed averaging model using the eigenvalue theorem (Fig. 4). Here, the phase plane analysis is not needed to verify the V_b responses again. The V_b responses adhere to the MIL-STD-704F standard because the sufficiently small K_{FB} was selected on the basis of the above-explained analysis in Fig. 5. The instability line is investigated from the unstable point ($P_{CPL} = 1.4$ kW) to the operating point at the rated power ($P_{CPL(rated)} = 2.2$ kW). Points ① to ④ of Fig. 4 for a given K_{FB} are located on the black dashed line of Fig. 7. The red and blue lines are defined via the first- and second-order polynomial fitting functions using function "polyfit" in MATLAB, respectively. The second-order polynomial equation is more accurate than the first-order polynomial equation. The blue line is fitted using (9), where a suitable K_{FB} can be adopted based on the P_{CPL} level.

$$K_{FB} = \left(-4.282\times10^{-7}\right)P_{CPL}^2 + 0.003P_{CPL} - 3.079 \qquad (9)$$

where $P_{CPL} = I_o V_b - \dfrac{V_b^2}{R_L}$

The blue area in Fig. 1 indicates the proposed adaptive stabilization for the MEA power system using (9). The P_{CPL} value for adapting the K_{FB} is calculated from I_o and V_b. Both values are measured from the existing current and voltage sensors. Additionally, (9) is only added to the code and operated when including the loop-cancellation technique. Consequently, the system is always stable until the rated power can be achieved. The K_{FB} varies when P_{CPL} changes.

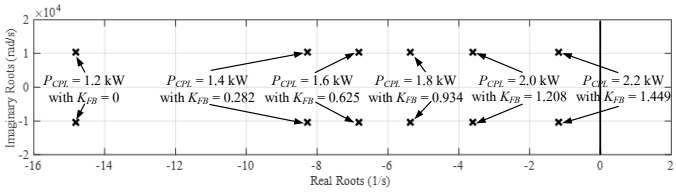

Fig. 8. Analytical results for the adaptive stabilization.

Fig. 8 shows the analytical results of adaptive stabilization via the dominant eigenvalue plots. It demonstrates that the real roots of the dominant eigenvalues with the adaptable K_{FB} are always on the left-hand side of the s-plane. The K_{FB} is slightly increased following the proposed adaptive equation in (9) until K_{FB} is equal to 1.449 at the rated power of 2.2 kW. It can be concluded that, before applying the proposed adaptive stabilization, the system becomes unstable at $P_{CPL} = 1.4$ kW (<rated power). After applying the proposed loop-cancellation technique using a simple equation, the appropriate K_{FB} is introduced into the system and, consequently, the system can be operated at the rated power.

IV. Simulation and Experimental Validation

In this section, the validation of the theoretical analysis by MATLAB simulation is presented alongside the details of the

experiment. A test rig of the considered MEA power system was designed and built in a laboratory (see Fig. 9). In this case, a programmable AC power supply was used rather than a PMSG, and the controlled buck converter was applied to represent the CPL.

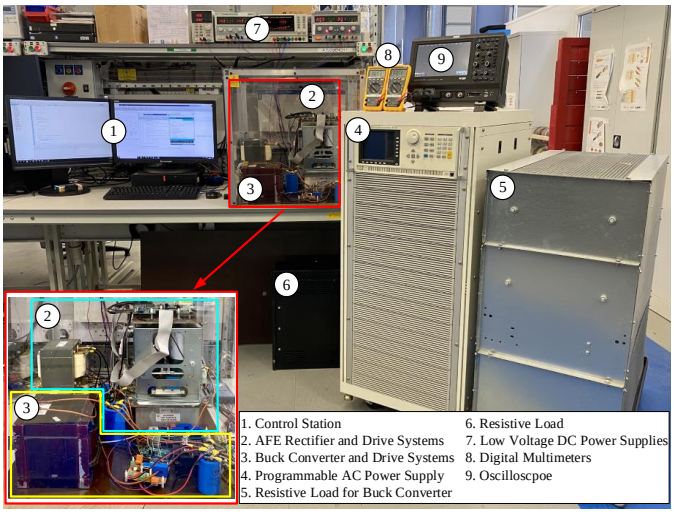

Fig. 9. Overview of the experimental setup.

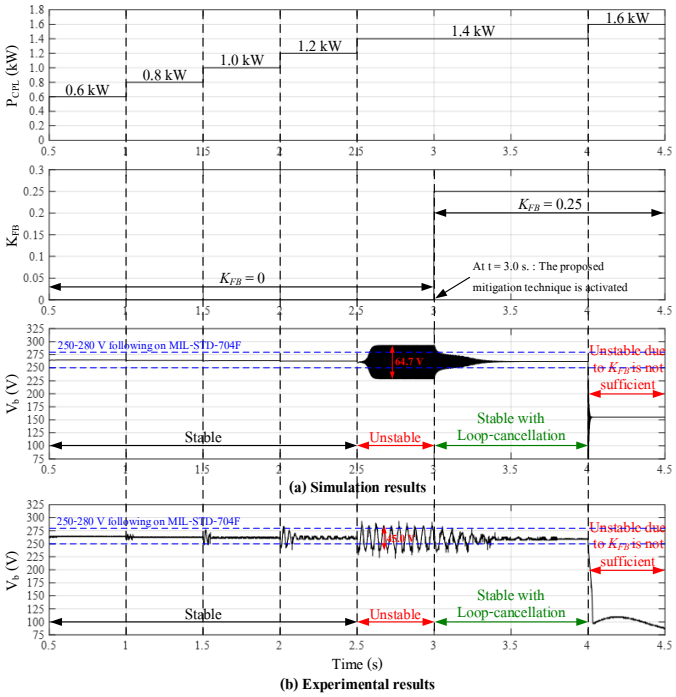

Fig. 10. Validation of the unstable point prediction and instability mitigation.

Fig. 10 shows the simulation and experimental results for the unstable point prediction and instability mitigation. Both the simulation and experimental results were tested in the same conditions and are summarized below.

- Initially, the system is operated without the proposed mitigation technique. The K_{FB} is designated as 0, and the P_{CPL} is increased by 200 W increments.

- At t = 2.5 s., the P_{CPL} is increased to 1.4 kW. As predicted by the analysis in Fig. 4(a) and Fig. 5(a), the system becomes unstable. Both the simulation results in Fig. 10(a) and the experimental results in Fig. 10(b) demonstrates the huge oscillation of V_b, which is not constant within the range of 250–280 V, as specified by the MIL-STD-704F standard. Furthermore, it has a ripple voltage equal to 67.4 V in the simulation and 45 V in the experiment, which does not follow the standard specifying the maximum ripple voltage in the steady-state (not exceeding 6 V). This indicates that the analytical, simulation, and experimental results are consistent in their indications that the system is unstable at this operating point.

- At t = 3.0 s., the proposed mitigation technique is activated. The K_{FB} is designated equal to 0.25. The unstable system at P_{CPL} = 1.4 kW returns to a stable state, denoted by the oscillation of V_b decreasing until it is constant within the range of 250–280 V in the steady-state, thereby adhering to the standard. This confirms that the proposed mitigation technique can return the unstable system to a stable state.

- Finally, at t = 4.0 s, the P_{CPL} is again increased to 1.6 kW while the K_{FB} is fixed at 0.25. The analytical results in Fig. 4(b) show that the dominant eigenvalues at this operating point are on the right-hand side of the s-plane. This indicates that the system is yet again unstable due to K_{FB} being insufficient for mitigation. Both the simulation results in Fig. 10(a) and the experimental results in Fig. 10(b) correspond to the analytical results in which the system is unstable. However, the system instability at this point V_b suddenly decreases without oscillation until the system fails. The system controllers will attempt to stabilize a system with insufficient K_{FB}, resulting in the modulation index reaching the limit specified for avoiding over-modulation. Consequently, the system will fail and will be unable to continue operating, which is an undesirable aviation situation. This confirms the conclusion that if P_{CPL} is increased, the K_{FB} must be increased to be appropriate for mitigation and to maintain system stability. Therefore, adaptive stabilization based on the P_{CPL} level is required.

Fig. 11 the confirmation results for the adaptive stabilization as expected from the analysis in Fig. 8, the system with an adaptable K_{FB} based on the P_{CPL} level (acquired using the proposed equation in (9)) is always stable for all P_{CPL} levels within the rated power. Both the simulation results in Fig. 11(a) and the experimental results in Fig. 11(b) confirm that the system is always stable and can be operated at the rated power, which can be observed as a result of V_b in the steady-state being constant within the range of 250–280 V as per the denoted standard. Although V_b in the experiment indicated a degree of ripple voltage, the maximum ripple voltage in the steady-state was <6 V and, as such, adheres to the denoted standard. In addition, the transient responses V_b from the simulation and experiment are shown in the zoomed area of Fig. 11(a) and Fig. 11(b). The responses have settling time = 0.02 s. (not exceeding 0.04 s.) without the overvoltage and undervoltage more than 330 V and less than 200 V, respectively, of which the results can also follow the standard.

This article has been accepted for publication in a future issue of this journal, but has not been fully edited. Content may change prior to final publication. Citation information: DOI 10.1109/TTE.2021.3081161, IEEE Transactions on Transportation Electrification

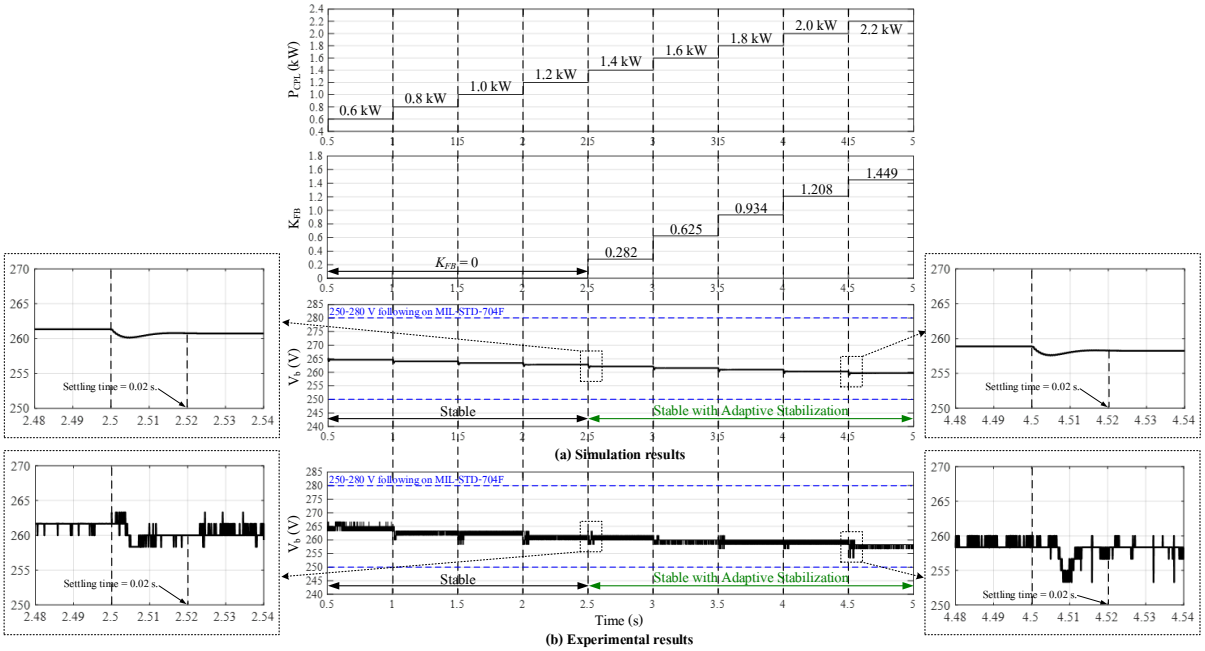

Fig. 11. Validation of the adaptive stabilization.

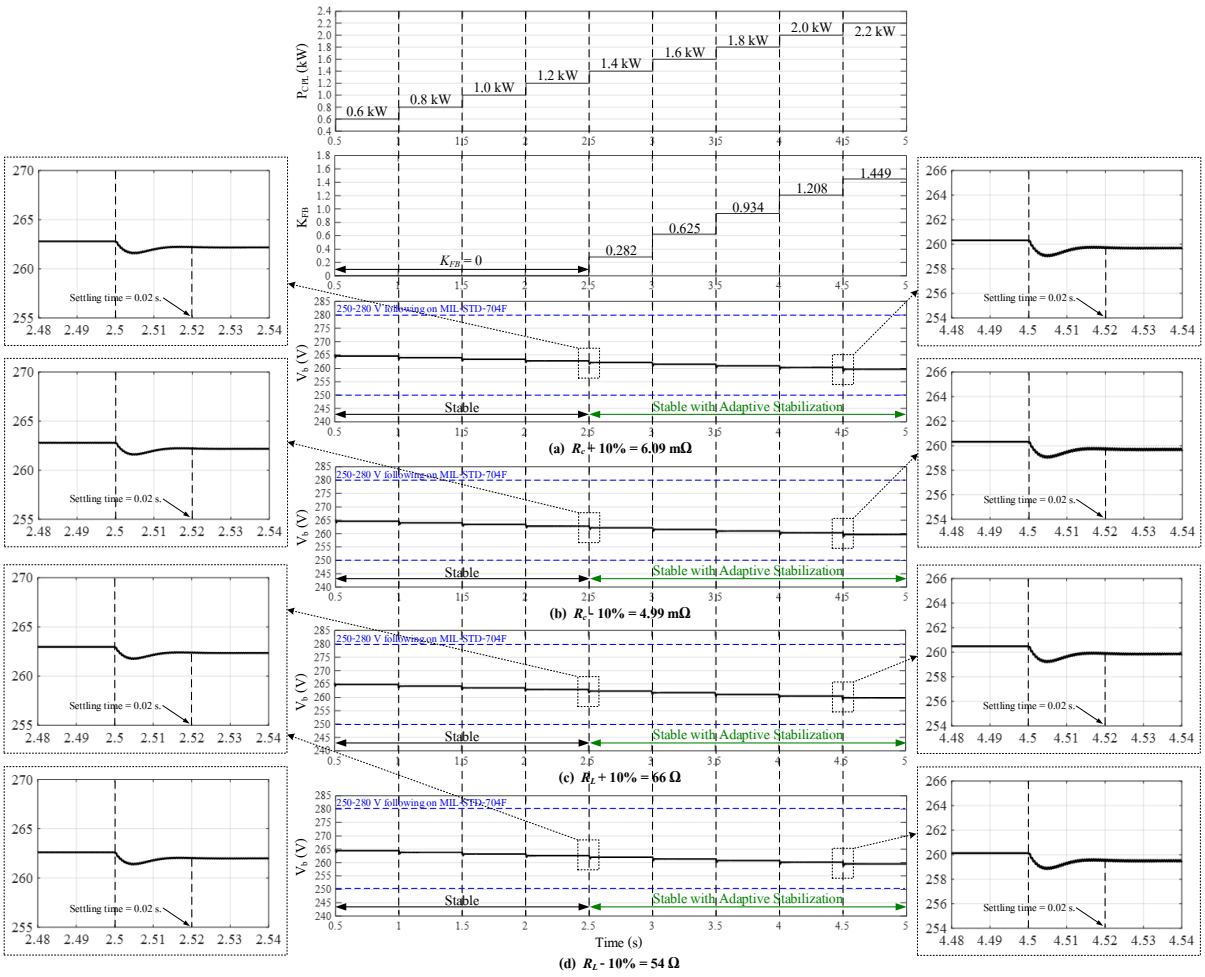

Fig. 12. Simulation results for the validation of the robustness of the proposed adaptive stabilization.

The simulation results using the proposed adaptive stabilization equation when R_c and R_L are changed to R_c + 10% = 6.09 mΩ , R_c - 10% = 4.99 mΩ , R_L + 10% = 66 Ω and R_L - 10% = 54 Ω are shown in Fig. 12(a) to Fig. 12(d), respectively. Although R_c and R_L changes, the system remains stable for all operating conditions within the rated power.

Moreover, the transient and steady-state responses V_b adhere to the MIL-STD-704F standard. This means that parameter robustness does not affect the adaptive stabilization results.

Overall it can be concluded that there is very good agreement between the analytical, simulation, and experimental results. Typically, a system without proposed adaptive stabilization will become unstable at $P_{CPL} = 1.4$ kW (<rated power). After applying the proposed adaptive stabilization approach based on the loop-cancellation technique and including the simple K_{FB} equation, which is defined using the proposed mathematical model including the eigenvalue theorem, system instability due to the CPL effect can be fully eliminated. Accordingly, the system always remains stable for all operating conditions within the rated power, i.e., $P_{CPL(rated)} = 2.2$ kW. As such, it is confirmed that the proposed adaptive stabilization is an effective approach that can be used to guarantee the stable operation of a PMSG-based DC electrical power system in a MEA.

V. Conclusions

This study presented an adaptive stabilization of a PMSG-based DC electrical power system in a MEA. The proposed approach is based on the loop-cancellation technique with a simple equation that can calculate the adaptable gain based on the relevant power level. This simple equation was derived from the polynomial curve fitting based on the proposed mathematical model. The resulting adaptive stabilization can eliminate system instability owing to the CPL effect. Consequently, the considered MEA power system is always stable and can be operated at the rated power. The theoretical analysis results (derived via the linearization technique with the eigenvalue theorem and the phase plane analysis), the simulation, and the experimental results used for results' validation, were consistent. The results confirm that the system is stable for all operating conditions within the rated power using the proposed adaptive stabilization without adding any equipment into the system. Also, the V_b response adheres to the MIL-STD-704F standard, and the parameter robustness within $\pm 10\%$ does not affect the adaptive stabilization results. Consequently, the proposed adaptive stabilization can effectively guarantee a PMSG-based DC electrical power system's stable operation in a MEA. However, the equation for calculating the proposed approach's adaptive gain is defined from the polynomial curve fitting based on the eigenvalue plot using the proposed model. If the system parameters are changed, the process of defining the adaptive stabilization equation is repeated following the summarized procedure in Fig. 13. First, a sufficiently small K_{FB} is defined for each P_{CPL} within the rated power via the stability analysis. Then, the instability line is calculated from the stability analysis results and used for polynomial curve fitting. The polynomial curve fitting is performed until the polynomial equation is equivalent to the instability line. Consequently, the adaptive stabilization equation is defined. Thus, in this context, providing the proposed adaptive stabilization represents a convenient and flexible approach, whereas a general and simple equation of K_{FB} can be developed in future studies. Moreover, adaptive stabilization for a realistic potential architecture of MEA, multi-generator(PMSGs)-single-bus DC distribution MEA power systems can also be considered.

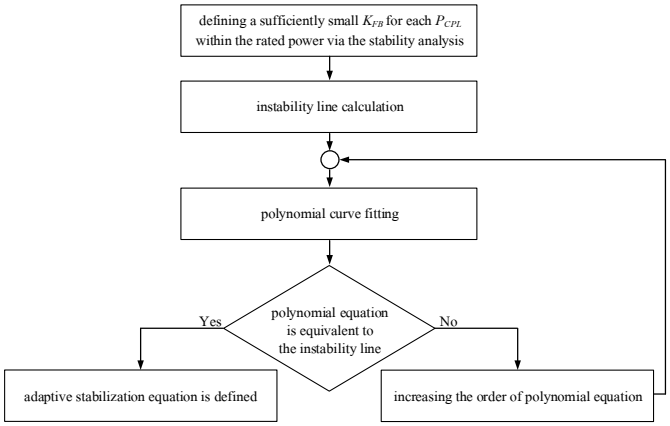

Fig. 13. Process flowchart for defining the adaptive stabilization equation.

Appendix

The System Parameters: $V_S = 100\ \mathrm{V_{rms/phase}}$, $f_e = 400$ Hz, $R_{AC} = 0.7\ \Omega$, $L_{AC} = 2$ mH, $C_{dc} = 1.45$ mF, $R_c = 5.54\ \mathrm{m\Omega}$, $L_c = 16.34\ \mu$H, $C_b = 0.99$ mF, $R_L = 60\ \Omega$, $V_{ds}^* = 0$ V, $V_o^* = 270$ V, $I_d^* = 0$ A, $K_D = 0.8$, $K_{pv} = 1.288$, $K_{iv} = 343.462$, $K_{pd} = K_{pq} = 17.069$, $K_{id} = K_{iq} = 78956.835$, $L_{Buck} = 5.094$ mH, $C_{Buck} = 474.1\ \mu$F, $R_{Buck} = 8.1\ \Omega$, $P_{CPL(rated)} = 2.2$ kW

Acknowledgment

This work was supported by the Thailand Research Fund (TRF), the Royal Golden Jubilee Ph.D. Program (RGJ: grant number PHD/0089/2560) and by Suranaree University of Technology (SUT), THAILAND and Institute for Aerospace Technology (IAT), University of Nottingham (UoN), UK.

References

[1] J. A. Rosero, J. A. Ortaga, E. Aldabas, and L. Romeral, "Moving towards a more electric aircraft," *IEEE Aerosp. Electron. Syst. Mag.*, vol. 22, no. 3, pp. 3-9, Mar. 2007.

[2] P. Wheeler, and S. Bozhko, "The more electric aircraft: technology and challenge," *IEEE Electrif. Mag.*, vol. 2, no. 4, pp. 6-12, Dec. 2014.

[3] F. Gao, S. Bozhko, A. Costabeber, G. Asher, and P. Wheeler, "Control design and voltage stability analysis of a droop-controlled electrical power system for more electric aircraft," *IEEE Trans. Indust. Electron.*, vol. 64, no. 12, pp. 9271-9281, Dec. 2017.

[4] F. Gao, X. Zheng, S. Bozhko, C. Hill, and G. Asher, "Modal analysis of a PMSG-based dc electrical power system in the more electric aircraft using eigenvalues sensitivity," *IEEE Trans. Transp. Electrif.*, vol. 1, no. 1, pp. 65-76, Jan. 2015.

[5] F. Gao, and S. Bozhko, "Modeling and impedance analysis of a single DC bus based multiple-source multiple-load electrical power system," *IEEE Trans. Transp. Electrif.*, vol. 2, no. 3, pp. 335-346, Jan. 2016.

[6] K-N. Areerak, T. Wu, S. V. Bozhko, G. M. Asher, and D. W. P. Thomas, "Aircraft power system stability study including effect of voltage control and actuators dynamics," *IEEE Trans. Aerosp. Elcetron. Syst.*, vol. 47, no. 4, pp. 2574-2589, Oct. 2011.

[7] A. Emadi, B. Fahimi, and M. Ehsani, "On the concept of negative impedance instability in the more electric aircraft power systems with constant power loads," *Soc. Automotive Eng. J.*, pp. 689-699, 1999.

[8] A. Emadi, A. Khaligh, C. Rivetta, and G. Williamson, "Constant power loads and negative impedance instability in automotive system: Definition, modeling, stability, and control of power electronic converters and motor drives," *IEEE Trans. Veh. Technol.*, vol. 55, no. 4, pp. 1112-1125, Jul. 2006.

[9] A. Griffo, and J. Wang, "Large signal stability analysis of 'more electric' aircraft power system with constant power loads," *IEEE Aerosp. Electron. Syst. Mag.*, vol. 48, no. 1, pp. 477-489, Jan. 2012.

[10] M. Cespedes, L. Xing, and J. Sun, "Constant-power loads system stabilization by passive damping," *IEEE Trans. Power Electron.*, vol. 26, no. 7, pp. 1832-1836, Jul. 2011.

[11] D. K. Fulwani, and S. Singh, "Mitigation of negative impedance instabilities in dc distribution systems: A sliding mode control approach," in *Springer briefs in applied sciences and technology*, Springer Nature, 2016, pp. 12-28.

[12] A. Rahimi, and A. Emadi, "Active damping in dc/dc power electronic converters: A novel method to overcome the problems of constant power loads," *IEEE Trans. Ind. Electron.*, vol. 56, no. 5, pp. 1428-1439, May 2009.

[13] A. M. Rahimi G.A. Williamson, and A. Emadi, "Loop-cancellation technique: A novel nonlinear feedback to overcome the destabilizing effect of constant-power loads," *IEEE Trans. Veh. Technol.*, vol. 59, no. 2, pp. 650-661, Feb. 2010.

[14] M. Wu, and D.D. Lu, "A novel stabilization method of LC input filter with constant power loads without load performance compromise in dc microgrid," *IEEE Trans. Ind. Electron.*, vol. 62, no. 7, pp. 4552-4562, Jul. 2015.

[15] A.A.A. Radwan, and Y.R. Mohamed, "Linear active stabilization of converter-dominated dc microgrid," *IEEE Trans. Smart Grid*, vol. 3, no. 1, pp. 203-216, Mar. 2012.

[16] Y. Li, L.R. Vannorsdel, A.J. Zirger, M. Norris, and D. Makismovic, "Current mode control for boots converters with constant power loads," *IEEE Trans. Circuit Syst.*, vol. 59, no. 1, pp. 198-206, Jan. 2012.

[17] X. Zhang, L. Xu, Y. Li, Z. Zheng, and K. Wang, "Stabilization and assessment of interaction dynamics for more electric aircraft," in *Proc. IEEE Inter. Power Electron. And Motion Control Conf.*, Hefei, China, Jul. 2016, pp. 1-7.

[18] Y.R. Mohamed, A.A.A. Radwan, and T. Lee, "Decoupled reference voltage-based active dc-link stabilization for pmsm drives with tight-speed regulation," *IEEE Trans. Ind. Electron.*, vol. 59, no. 12, pp. 4523-4536, Dec. 2012.

[19] P. Magne, D. Marx, B. Nahid-Mobarakeh, and S. Pierfedrici, "Large-signal stabilization of a dc-link supplying a constant power load using a virtual capacitor: Impact on the domain of attraction," *IEEE Trans. Ind. Appl.*, vol. 48, no. 3, pp. 878-887, May 2012.

[20] P. Magne, B. Nahid-Mobarakeh, and S. Pierfedrici, "Active Stabilization of dc microgrids without remote sensors for more electric aircraft," *IEEE Trans. Ind. Appl.*, vol. 49, no. 5, pp. 2352-2360, Sep. 2013.

[21] Y. Huangfu, S. Pang, B. Nahid-Mobarakeh, L. Guo, A. K. Rathore, and F. Gao, "Stability analysis and active stabilization of on-board dc power converter system with input filter," *IEEE Trans. Ind. Electron.*, vol. 65, no. 1, pp. 790-799, Jan. 2018.

[22] F. Liu, L. Xu, R. Liu, and Y. Li, "Impedance and stability analysis of a permanent magnet synchronous generator system for more electric aircraft," *IEEE Int. Conf. on Electrical systems for Aircraft, Railway, Ship Propulsion and Road Vehicles & International transportation Electrification Conference (ESARS-ITEC)*, Nottingham, UK, Nov. 7-9, 2018.

[23] O. Lorzadeh, I. Lorzadeh, M.N. Soltani, and A. Hajizadeh, "A novel active stabilizer method for DC/DC power converter systems feeding constant power loads," *IEEE 28th International Symposium on Industrial Electronics (ISIE)*, Vancouver, BC, Canada, June 12-14, 2019.

[24] S. Pang, B. Nahid-Mobarakeh, S. Pierfederici, Y. Huangfu, G. Luo, and F. Gao, "Towards stabilization of constant power loads using IDA-PBC for cascaded LC filter DC/DC converters," *IEEE Journal of Emerging and Selected Topics in Power Electronics.*, vol. 1, no. 1, pp. 1-12, Oct. 2019.

[25] S. Pang, B. Nahid-Mobarakeh, S. Pierfederici, M. Phattanasak, Y. Huangfu, G. Luo, and F. Gao, "Interconnection and damping assignment passivity-based control applied to on-board DC-DC power converter system supplying constant power load," *IEEE Trans. Indust. Appli.*, vol. 55, no. 6, pp. 6476-6485, Dec. 2019.

[26] T. Sopapirm, K-N. Areerak, S. Bozhko, C. Hill, A. Suyapan, and K-L. Areerak, "Adaptive stabilization of uncontrolled rectifier based ac-dc power systems feeding constant power loads," *IEEE Trans. Power Electron.*, vol. 33, no. 10, pp. 8927-8935, Oct. 2018.

[27] MIL-STD-704F Standard, Department of defense interface standard, Aircraft electric power characteristic, http://www.dodssp.daps.mil/.

Apichai Suyapan was born in Chiang Mai, Thailand, in 1991. He received the B.Eng. (first-class honors), and M.Eng. degrees in electrical engineering from Suranaree University of Technology (SUT), Nakhon Ratchasima, Thailand, in 2013 and 2016, respectively, where he is currently studying toward the Ph.D. degree in electrical engineering. From March 2019 to March 2020, he was a visiting student for conducting a short term research at Institute for Aerospace Technology (IAT), University of Nottingham, Nottingham, United Kingdom. His main research interests include stability analysis of power systems with constant power loads, modeling and control of power electronic based systems, and control theory.

Kongpan Areerak (M'16) received the B.Eng. and M.Eng. degrees from Suranaree University of Technology (SUT), Nakhon Ratchasima, Thailand, in 2000 and 2001, respectively and the Ph.D. degree from the University of Nottingham, Nottingham, United Kingdom, in 2009, all in electrical engineering. In 2002, he was a Lecturer in the Electrical and Electronic Department, Rangsit University, Thailand. Since 2003, he has been a Lecturer in School of Electrical Engineering, SUT. He has received the Associate Professor in Electrical Engineering since 2015. His main research interests include system identifications, artificial intelligence applications, stability analysis of power systems with constant power loads, modeling and control of power electronic based systems, and control theory.

Serhiy Bozhko (M'97-SM'18) received the M.Sc. and Ph.D. degree in electromechanical systems from the National Technical University of Ukraine, Kyiv City, Ukraine, in 1987 and 1994, respectively. Since 2000, he has been with the Power Electronics, Machines, and Controls Research Group, University of Nottingham, Nottingham, United Kingdom, where he is currently a Professor of Aircraft Electric Power Systems and the Director of the Institute for Aerospace Technology. He is leading several EU- and industry-funded projects in the area of aircraft electric power systems, including power generation, distribution and conversion, power quality, control and stability issues, power management and optimization, as well as advanced modeling and simulations methods.

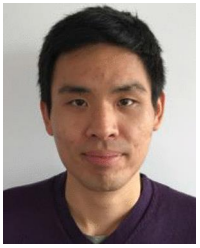

Seang Shen Yeoh received the M.Sc. degree (with distinction) in power electronics and the Ph.D. degree in electrical engineering from the University of Nottingham, Nottingham, United Kingdom, in 2011 and 2016, respectively. Since then, he has been a Research Fellow with the Power Electronics, Machines, and Controls Research Group, University of Nottingham. His current research interests include aircraft application, namely modeling and stability studies of complex power systems, and new control strategies for high-speed drive systems.

Kongpol Areerak received the B.Eng., M.Eng., and Ph.D. degrees in electrical engineering from Suranaree University of Technology (SUT), Thailand, in 2000, 2003, and 2007, respectively. Since 2007, he has been a Lecturer and Head of Power Quality Research Unit (PQRU) in the School of Electrical Engineering, SUT. He has received the Associate Professor in Electrical Engineering since 2015. His main research interests include active power filter, harmonic elimination, motor drive, AI application, and intelligence control system.